WATER BODY AREA MEASUREMENT FROM SATELLITE IMAGE USING DEEP LEARNING

Dr. Shofia Priyadharshini[1], R.Breesha[2], S.Mithun Varshan[3], M.Mari Perumal[4], S.Mani Kandan[5]

Abstract

For the planning and development of rural and urban areas, land cover segmentation of plant and water body areas from satellite images is essential. Large sample image datasets are needed for train the land cover categorization algorithms that are currently in use. Due to heterogeneous pixel as well as geometric distortion over boundaries and curvature zone, classifying the land cover of plant and water areas using existing algorithms is a difficult process. The accurate categorization and measuring of land cover are impacted by mixed pixels. Geometric distortion affects the contour of the land cover and results from the framing of isotropic and angular selectivity while image acquisition. Without training datasets, the intent of Transverse dyadic wavelet transform (TDyWT)[2] in this study improves and classifies the vegetation and water area in the land cover of LANDSAT images. The proposed TDyWT employs Cantor 5x9x7 wavelet for reconstructing and Haar wavelet for decomposition. Due to the wavelet's reversible and lifting qualities, the TDyWT improves the contour, curvature, and boundary[1] of plant and water areas in LANDSAT images. Geometric distortion and spatial scale[1] mistake of mixed pixels are eliminated by TDyWT. By total station and errors modelling methodologies, spatial scale inaccuracy in classic land surveying is eliminated. According to the findings, compared to ground truth survey methods, the introduced TDyWT algorithm identifies the area of subclasses of vegetative and water with 95% accuracy. The proposed approach was evaluated on a dataset of satellite images and achieved high accuracy in measuring water body areas. The results demonstrate the potential of deep learning methods for accurately and efficiently monitoring water resources from satellite imagery.

Keywords: Remote sensing • Land cover categorization• Geometric distortion•Transverse dyadic wavelet transform•Denoising Convolutional Neural Network

[1,2]Assistant Professor,Department of Electronics and Communication Engineering,Vel Tech High tech Dr.Rangarjan Dr.Sakunthala Engineering College, Chennai,India.
[3,4,5]UG Scholar,Department of Electronics and Communication Engineering,Vel Tech High tech Dr.Rangarjan Dr. Sakunthala Engineering College, Chennai,India.

1. Introduction

The technique of learning about an object or phenomenon without coming into direct contact with it is called remote sensing.This is typically done using sensors on aircraft or satellites that collect data in the form of images or other types of measurements. The info about the object or phenomena being investigated, which includes its region, size, shape, and composition, can then be gleaned from the data through analysis. Remote sensing is used in a wide range of fields, including geography, geology, agriculture, forestry, oceanography, and meteorology. One example of a remote sensing satellite is LANSAT.

The US Geological Survey launched and maintains a series of Earth observation satellites known as Landsat (USGS) and Kaggle earth images.Landsat 1, its first Landsat satellite, was launched in 1972, and Landsat 8, the most current, was launched in 2013.Instruments on board Landsat satellites acquire data in the electromagnetic spectrum's visible, infrared, and thermal infrared ranges. Images of the Earth's land surface are produced using this data, and these images can be used for a variety of purposes, including mapping natural resources, tracking changes in land use and land cover, and evaluating the condition of crops and forests.

The Landsat program is considered one of the longest-running civilian satellite programs and the imagery and data provided by it are freely available to the public.Geometric distortion refers to the deviation of the shape or size of an object in an image from its true shape or size. This can occur in remote sensing images due to a variety of factors, such as the sensor's design, the altitude of the sensor, and the terrain being image.Radial distortion and tangential distortion are the two basic categories of geometric distortion. When the distance between the sensor and the item being image is not constant, radial distortion occurs, making objects appear warped or curved.

Tangential distortion occurs when the sensor is not perpendicular to the object being image, causing the edges of the image to appear skewed or distorted.Geometric distortion can have a significant impact on the accuracy and usefulness of remote sensing images. It can make it difficult to accurately measure distances and sizes, and can also make it challenging to correctly identify and classify objects in the image. To correct for geometric distortion, various geometric correction techniques can be applied, such as polynomial correction and image rectification.

Geometric Distortion in Image Classification
Geometric distortion in remote sensing images can have a significant impact on image classification, which is the process of identifying and categorizing objects in an image.When geometric distortion is present, objects in the image may appear elongated, squashed, or skewed, making it difficult for a classifier to accurately identify and classify them. For example, a distorted image of a building may make it appear smaller or taller than it actually is, leading the classifier to misclassify it as a different type of structure.

Similarly, a distorted image of a forest may cause the classifier to miss some of the trees, leading to an underestimate of the forest cover.Applying geometric correction techniques to the image before classification is required to combat the impacts of geometric distortion on image classification. This can include techniques such as polynomial correction, image rectification, and sensor modeling.

These methods can help to increase the accuracy and dependability of image classification results by reducing the geometric distortion.It's also worth noting that some image classification algorithms are more robust to geometric distortion than others, for example, deep learning-based classifiers are known for their robustness to different image distortions, due to the large amount of data they are trained on.
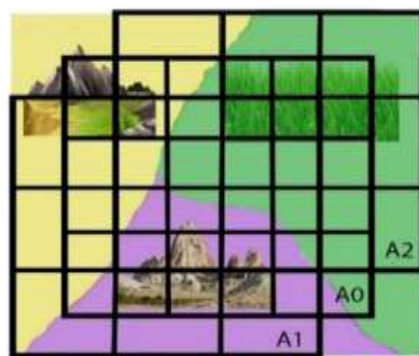

Fig 1 Geometric error in boundary regions.

The earth's rotation, scan skew, satellite velocity, mirror scan velocity of the image sensor, and aspect ratio all contribute to systematic inaccuracy.

Ground swath is anomalous during image capture, and scan skew, which results from the rotational movement of the satellite, emerges. In LANDSAT,

Eur. Chem. Bull. 2023, 12 (S3), 1518 – 1530

1519

the N-S axis is the source of skew, and the skew angle is measuredas in Eq. (1).

$$\theta = 90 - \cos^{-1} 1 = \sin(\theta e)/\cos(L) \qquad (1)$$

θ e = The satellite's forward motion's direction.

L = Latitude where the skew angle should be calculated.

Figure 1 shows the satellite image's boundary regions' geometric errors in graphic form. Track scale distortion results from variations in satellite velocity. The scan distortion is caused by the earth's rotation while satellite images are being scanned. The orbiting satellite surveys the surface of the planet while rotating at a speed proportional to nadir.The lines of longitude and the start and end scan lines are always aligned in a LANDSAT image, and there is never any skew. improperly slow image sensor scanning speed.The geometric distortion is caused by LANDSAT's slow scan velocity and long scan time. The pixel provided by the LANDSAT multispectral scanner system (MSS) is not square because to oversampling along

the scanning tracks, which causes space between the pixel region. The matrix below displays the region with uneven pixels and spacing.

$$A = \begin{bmatrix} 0.0 & 1.41 \\ 1.0 & 0.00 \end{bmatrix} \qquad (2)$$

Due to oversampling, pixel 1.0's value in the matrix differs from 1.41.

Satellite Image With Mixed Pixels

When more than one form of land cover or land use is combined into a single pixel on an image taken by a satellite, it is known as a mixed pixel. This can occur when several land cover categories are present in a single pixel or when the pixel size of the satellite data is insufficient to differentiate specific features on the ground.This can make it challenging to accurately classify or interpret the image, and may require specialized techniques such as spectral unmixing or sub-pixel mapping to account for mixed pixels.
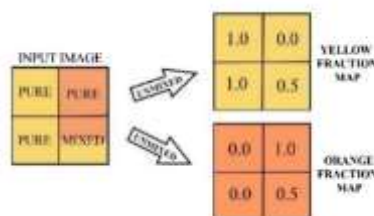

Fig 2 Mixed pixel in satellite image

Related Work

The medium-resolution spectral imager (MERSI) sensor aboard the FY3A meteorological satellite is used to capture images. The normalised index classifies water bodies using the FY3A picture(Long et al. **2009**). Moreover, SAR images are utilised to classify water bodies using a variety of techniques, including back scatter for water mask refining, advanced morphological filtering, and coarse water mask identification (Zeng et al. **2015**). Also, the classification of urban and vegetated areas is done statistically using the support vector machine (SVM), maximum likelihood (ML), and artificial neural network techniques (ANN).

SVM performs better than ML and ANN for classifying urban and vegetative areas in satellite images (Pal and Mather **2005**).To categorise buildings and trees, LIDAR satellite images are employed (Zarea and Mohammadzadeh**2016**). The SVM approach uses colour and texture features to classify different kinds in the LIDAR image, including vegetation, buildings, and urban areas (Harbas and Subasic**2014**). Also, hiimage detects high-density vegetation in urban area using the SVM approach (Iovan et al. **2008**). With a multi-level context framework, the SVM approach categorises the high-dimensional characteristic in

high-resolution satellite images (Bruzzone and Carlin **2006**). Moreover, naïve Bayes' (Zhan and Lai **2012**) and scale-invariant feature transform (SIFT) (Sirmacek and Unsalan**2009**) Algorithm recognises vegetation and urban areas, although vegetation areas are only efficiently classified when graph theory and SIFT are combined.

Nevertheless, due to the irregular area and spatial error that occur during measurement, the classification algorithm never distinguishes between the corner edge and geographic region in the urban area. For instance, assessment of the vegetation area between building areas includes the spatial error caused by mixed pixels because urban areas typically have vegetative cover in between the edifice areas. By using a weighted Gaussian voting matrix, the urban area categorization for vegetation between buildup areas is determined(Shi et al. **2015**). The above-mentioned algorithms classify plants and buildings using a manual process that introduces greater spatial error during measurement. However comparable classification is also carried out automatically using tools like the object-based threshold-free evaluation system (Awrangjeb and Fraser **2014**), Gabor filter and the best method for making decisions (Sirmacek and Unsalan**2010**), texture evaluation (Petrou et al. **2015**), Regression using support vectors (Fan et al.

2015), complicated wavelet transform with dual trees (Demirel and Anbarjafari**2010**), normalized vegetation index (NVI) (Blaschke et al. **2014**), and Using J-measure segmentation (Wang and Boesch**2007**).

Height of canopy model (CHM) (Paris et al. **2016**), models for ellipsoidal tree crowns (Lindberg et al. **2014**), the vegetation index for normalized differences (NDVI) (McInnes et al. **2015**), and algorithm for water surface boundary detecting (WSB-DA) (Singh et al. **2016**). The geometry distortion and mixed pixel are never eliminated by the automatic classification system, which leads to measurement error. Additionally, by using a local searching method, the improvement of perceptual salient boundaries in images can be used to calculate the intensity of directional vectors in the image space (Xie et al. **2006**) and created a level-set method for automatically segmenting the folded surface (Zhu et al. **2013**), is accomplished.

Moreover, the dyadic wavelet analysis preserves the image edges in a select few medical applications (Nageswari and Prabha**2018**). Based on reproducible kernel theory under greatly generalised differentiability, frizzy differential equations are resolved (Arqub et al. **2016**). Additionally, second-order, two-point frizzy boundary value problems are solved by kernel algorithms (Arqub et al**. 2017**). Framework of second-order boundary value issues are resolved by continuous genetic algorithm (CGA), where the necessary nodal values are generated from smooth solution curves (Arqub and Abo1)

Enhancement Algorithms For Satellite Image

For urban planning and development, land cover classification plays an important role for identification of temporal changes. Vegetation classes are forest, agriculture areas and reserved forest area. Government and non-governmental agencies needs land cover boundaries for various decision making such as road plan, deforestation and afforestation. For land cover measurement, satellite images with different resolutions are used for delineation and precise Vegetation and other places, like a water body, a road, a building, etc., are measured in terms of area. Researchers has developed various methods for automatically classifying different types of vegetation from high-resolution satellite pictures. Until now, support vector machines (SVM)[1] and neural network (NN)[1] algorithms used to delineate vegetation area. SVM, Frizzy, Bayesian, Linear, K-nearest Neighbors (KNN), and Quadratic are examples of existing classifiers that use object evaluation to distinguish between urban and vegetated areas.

The existing algorithms and classifiers such as SVM and Due to its quick processing, artificial neural networks (ANN) are used for vegetation classification, still accuracy in area measurement the vegetation is a difficult task. Classifiers perform worse and use more memory as a result of geometric distortion and mixed, unclassified pixels, which causes spatial inaccuracy in area measurement. Mixing pixels in a certain class cause area measurement errors across land areas with vegetation and water bodies.

In this thesis, three types of enhancement algorithms are proposed in a satellite image, to distinguish between vegetation and water body. They are

    i. Transverse Dyadic Wavelet Transform (TDyWT)
    ii. Stationary Wavelet Transform (SWT)
    iii. Dyadic Wavelet Transform (DWT)
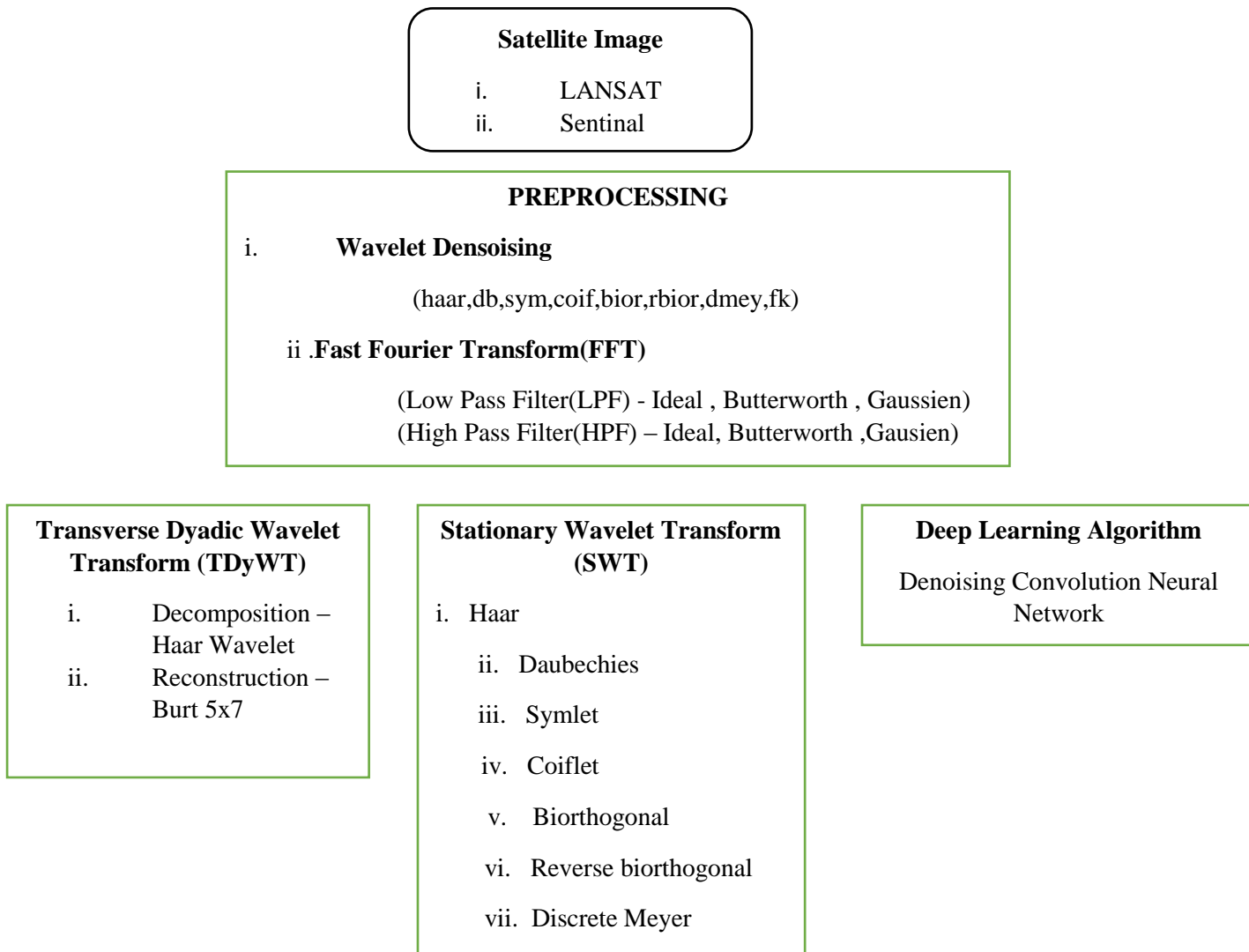   iv. Denoising Convolutional Neural Network (DnCNN)

Eur. Chem. Bull. 2023, 12 (S3), 1518 – 1530

1521

Satellite Image

i.   LANSAT
ii.   Sentinal

PREPROCESSING

i.   **Wavelet Densoising**

(haar,db,sym,coif,bior,rbior,dmey,fk)

ii .**Fast Fourier Transform(FFT)**

(Low Pass Filter(LPF) - Ideal , Butterworth , Gaussien)
(High Pass Filter(HPF) – Ideal, Butterworth ,Gausien)

Transverse Dyadic Wavelet Transform (TDyWT)

i.   Decomposition – Haar Wavelet
ii.   Reconstruction – Burt 5x7

Stationary Wavelet Transform (SWT)

i.   Haar

ii.   Daubechies

iii.   Symlet

iv.   Coiflet

v.   Biorthogonal

vi.   Reverse biorthogonal

vii.   Discrete Meyer

Deep Learning Algorithm

Denoising Convolution Neural Network

Fig 3 Proposed Methodology

LANSAT image

R-Band
G-Band
B-Band

Dyadic Transform (Removes Distortion)

(i)   Haar Wavelet-Decompose (Preserveedges

(ii)   Reversible Property

Inverse Dyadic Transform

(i)Burt 5x7 wavelet transform– Reconstruct (Perspective projection-remove mixwd pixel

(ii)Lifting property

R-Band
G-band
B-Band

Band Combination

(i)Preserve boundary and edges (ii)Perspective projection of boundary eliminate geometric region
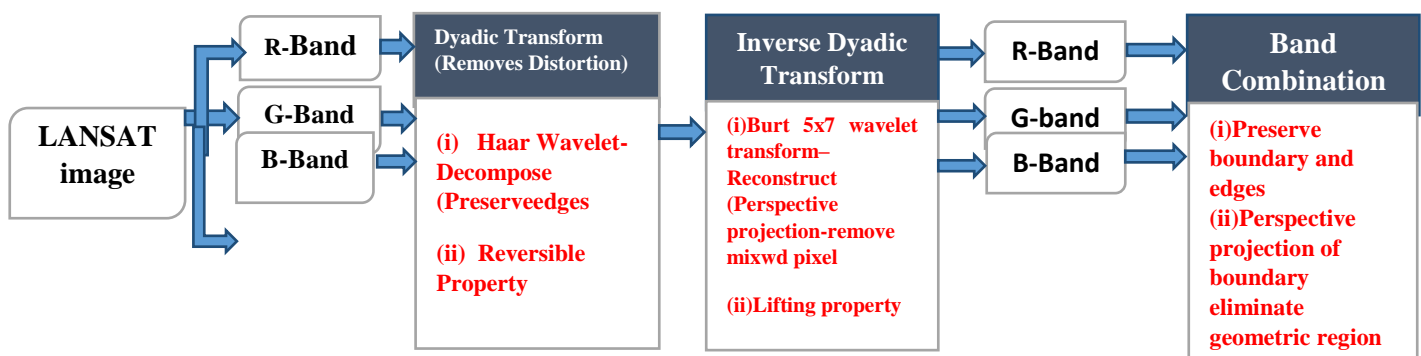
Fig 4 Workflow of Proposed Methodology

Wavelet Dyadic Transform
In order to create a dyadic wavelet, mother wavelet and dyadic deforms convolve. The term "dyadic wavelet transformation" in Eq. (3)

$$Wf(u, 2^j) = \int_{-\infty}^{\infty} f(t) \frac{1}{2} \Psi \left(\frac{t-u}{2^j} \right) dt = f * \psi_2 j(u)$$

(3)

As a function with zero meaning, let's Ψ call it the mother wavelet. Level j-level dilation is shown in Eq. (4)

$$\psi_{2^j}(x) = \frac{1}{2^j} \psi \left(\frac{x}{2^j} \right)$$ (4)

The definition of the wavelet transform of f(x) at the dyadic scale j and position x in Eq. (5)

$$w_{2^j}f(x) = f * \psi_{2^j}(x) = \int f(t) \cdot \psi_{2^j}(x - t)\, dt \quad (5)$$

A rescaled square shape function has been added to the dyadic wavelet transform's sequence as in Eq. (6)

$$W_f = \left(W_{2^j}f(x)\right)_{j \in Z} \quad (6)$$

The wavelet transform operator for dyads is W
W2 j f(x) (x) is W2 f (xFourier)'s transform, as in Eq. (7)

$$\hat{W}_{2^j}f(x) = \hat{f}(w)\hat{\psi}(2^j) \quad (7)$$

If □ω ε Z the values of the positive constants A1 and B1 in Eq. (8)

$$A_1 \le \sum_{-\infty}^{\infty} \left|\hat{\psi}(2^j w)\right|^2 \le B \quad (8)$$

As a result of the dilation of (w) by (2j)jZ throughout the entire frequency axis, the dyadic wavelet transform reconstructs as f(x) in Eq (9). The wavelet that was rebuilt has the property of v(x), and its Fourier transform meets the criteria listed belowas in Eq. (10)

$$\sum_{j=-\infty}^{\infty} \hat{\Psi}(2^j w)\hat{\chi}(2^j w) = 1 \quad (9)$$

using the infinite summation, f(x) was reconstructed as

$$f(x) = \sum_{j=-\infty}^{\infty} W_{2^j}f * \chi_{2^j}(w) \quad (10)$$

sequence (gj(x))jZ, with W-1 standing for the inverse dyadic wavelet transform operator , defined as in Eq. (11)

$$W^{-1}\left(g_j(x)\right)_{j \in Z} = \sum_{-\infty}^{\infty} g_{j*}\chi_{2^j}(w) \quad (11)$$

(gj(x))j∈Zonly if it fulfils the dyadic wavelet transform function in L2(R) Eq. (12)

$$W\left(w^{-1}g_1(x)\right)_{j \in Z} = \left(g_j(x)\right)_{j \in Z} \quad (12)$$

gj(x)∈ L²(R)be dyadic wavelet of function in L2 never necessarily (R).

If the aforementioned criterion is met by the sequence, the function creates the dyadic wavelet transform.

Transverse Dyadic Wavelet Transform
The LANDSAT image of different city is used in this study to test the proposed TDyWT, which consists of the Haar wavelet for decomposition and the Burt 5 x 7 wavelet for reconstruction. The calculation of the Haar wavelet is quick and never needs a temporary array. A series of "square shaped" functions that have been scaled down are used to create the Haar wavelet. As the Haar wavelet is not continuous, it can never be differentiated.
The ψ wavelet alters the mother wavelet, which is as in Eq. (13)

$$[W_\Psi f](a, b) = \frac{1}{\sqrt{|a|}} \int_{-\infty}^{\infty} \overline{\Psi\left(\frac{(x-b)}{a}\right)} f(x)\, dx \quad (13)$$

Cjk = wf, the wavelet coefficient (2-j,k2-j). Dyadic dilation (or binary dilation) is the process of finding a = 2-j. The binary or dyadic position of b = k2-j.

The mother wavelet function ψ(t) of the Haar wavelet is shown as in Eq. (14)

$$\Psi(t) = \begin{cases} 1 & 0 \le t < \frac{1}{2} \\ -1 & \frac{1}{2} \le t < 1 \\ 0 & otherwise \end{cases} \quad (14)$$

The scale function u(t) is shown as in Eq. (15)

$$\varphi(t) = \begin{cases} 1 & 0 \le t < 1 \\ 0 & otherwise \end{cases} \quad (15)$$

On the real line R, the Haar function is defined for each pair of integers n, k in Z as in Eq. (16)

$$\psi_{n \cdot k}(t) = 2^{n/2}\psi_{(2^n t - k), t \in R} \quad (16)$$

The right-optional interval In,k = [k 2-n, (k + 1) 2-n] supports the above function as in Eq. (17)

$$\int_R \Psi_{n \cdot k}(t)\, dt = 0, \|\Psi\|_{L^2}^2(R) = \int_R \psi_{n \cdot k}(t)^2\, dt = 1 \quad (17)$$

Haar function is an orthogonal pair function as in Eq. (18)

$$\int_R \psi_{n_{1,k_1}}(t)\psi_{n_2,k_2}(t)dt = \delta_{n_{1,k_1}}\delta_{n_2,k_2} \quad (18)$$

The set of function for the real line is calledHaaras in Eq. (19)

$$\{\Psi_{n,k}(t); n \in Z, K \in z\} \quad (19)$$

Burt function, also known as pyramidal coding, does multi-resolution analysis and is quite similar to sub-band coding. {ψt : l = 1; ...M -1} as in Eq. (20)

$$\psi_{j,k,l}(\cdot) = 2^{j/2}\psi_l(2^j - k) \quad (20)$$

As in Eq., the following orthogonality connection is met Eq(21)

$$\langle \psi_{j,k,l}, \psi_{j^1,k^1,l^1} \rangle = \delta_{j,j^1}\delta_{k,k^1}\delta_{l,l^1} \quad (21)$$

In this study, the LANDSAT picture is transformed using the Burt 5 x 7 wavelet during construction and the Haar wavelet during wavelet transverse dyadic wavelet transformation (TDyWT). Discrete wavelet transform uses a similar wavelet transform for deconstruction and rebuilding. The image is subbanded N times in a discrete wavelet transformation, where N represents the total number of subdivisions. In contrast to the dyadic transformation, the discrete wavelet transform (DWT) has a sub-band level N of 4 instead of 2. The dyadic wavelet transform's tensor product is 2*2 = 4. The dyadic wavelet transform torus product can be isolated as opposed to the DWTThe quantity of contrast and colour in the LANDSAT image depends on how much sub-band N a dyadic wavelet decomposes. More characteristics are conserved in the Landsat tm since the dyadic transform uses fewer sub-bands. The mother wavelet has been enlarged by powers of two in a dyadic wavelet transformation to remove the distortions from the image. In this method, scale samples of the wavelet transformation are ordered geometrically in a ratio of 2.

In the recommended approach for increasing the curvature and limits of water bodies

Eur. Chem. Bull. 2023, 12 (S3), 1518 – 1530

1523

and vegetation with perspective projection on the borders and outline of land classes, the transverse dyadic wavelet forms with Haar and Burt 5 x 7. The Haar wavelet has the property of being reversible during decomposition, maintaining the edge and contours. The Haar wavelet calculates the average and difference on each pair of pixel values, shifts the two values, and then calculates the average and differences of the succeeding pixel value in order to precisely capture all high-frequency changes.All high-frequency alterations are preserved in their reflection, and the edge and border are undamaged after decaying. The Burt 5 x 7 wavelet's mixed pixel and geometrical distortions are removed by the transverse wavelet, which also uses perspective projections to improve the border and curvature. The lifting property of the transform alternately applies to both horizontal lifting and vertical lifting, as predicted by the local windows for high-pixel correlation. This rich orientation causes the image pixels in the local windows to exhibit the perspective projection in the boundary and curvature of the land class. As a result of the lifting, the mixed pixel is removed from the LANDSAT image, allowing the fractional pixel accuracy level to maintain high resolution and retain the right reconstruction during the perspective projection of the pixel in the edges and border.

Wavelet Transform in Stationary Mode (SWT)
The Wavelet Transform in Stationary Mode (SWT)is a signal processing technique used for time-frequency analysis of signals. It decomposes a given signal into a set of wavelet coefficients, which provide details regarding the signal's frequency content at different period scales.The mathematical formulation of the SWT involves a multi-resolution signal analysis using wavelets. Given a signal x(t), the SWT can be obtained as follows:
Choose a wavelet function, which is typically a finite-length, oscillatory waveform that is localized in both time and frequency. Let us denote the wavelet function by ψ(t).
Generate a scaled and translating wavelet family by dilating and shifting the wavelet function. The scaled and translated wavelets are stated by

$$\Psi^{-\{j^*,k\}}(t) = 2^{(j/2)/\pi(2^{jt-k})}$$

where j and k are integer parameters that control the scale and position of the wavelet, respectively.
Compute by combining the signal with the scaled and translated wavelet coefficients at each scale j and position k wavelets
W j,k = langle x(t), psi j,k(t), where langlecdot, cdotrangle stands for the inner product.Apply a low-pass filter to the signal and downsample it by a factor of 2to obtain a coarser version of the signal. This process is repeated at each scale to obtain a set of wavelet coefficients that are localized in time

and frequency.The resulting wavelet coefficients provide a representation of the signal that captures its time-frequency content at different scales. The SWT can be inverted to reconstruct the signal from its wavelet coefficients, which allows for efficient compression and denoising of signals.

Denoising Convolutional Neural Network (DnCNN)
The Denoising Convolutional Neural Network (DnCNN) is a type of deep learning model that is designed to remove noise from images. In mathematical terms, DnCNNis conceivable as a mapping function. F: X → Y, where X is the set of noisy images and Y is the set of clean images. DnCNN consists of multiple layers of Convolutional neural networks are employed to identify the characteristics of noisy images. Each layer's output is run through an activation function such as ReLU (rectified linear unit) to introduce non-linearity. The output of the last layer is the estimated clean image, which is obtained by reducing a loss function that gauges how much the estimated clean picture differs from the actual clean image. The training of DnCNN involves minimizing the between the estimated clean picture and the actual clean image, the mean squared error (MSE). This can be expressed as: The Denoising Convolutional Neural Network (DnCNN) is a one of the type of deep learning model that is designed to remove noise from images. In mathematical terms, A mapping function F: X → Y, where X is the set of noisy images and Y is the set of clean images, can be used to represent DnCNN.
DnCNN consists of multiple layers of Convolutional neural networks are employed to identify the characteristics of noisy images. Each layer's output is run through an activation function such as ReLU (rectified linear unit) to introduce non-linearity. The output of the last layer is the estimated clean image, which is obtained by reducing a loss function that gauges how much the estimated clean picture differs from the actual clean image. The training of DnCNN involves reducing the mean squared difference (MSE) between the estimated and real clean image. The formula for this is:minimise ‖F(x) - y‖2.
where y corresponds to the ground truth clean image for an image that is noisy (x), and F(x) is the estimated clean image obtained by the DnCNN, and ‖.‖^2 represents the L2 norm. During testing, given a noisy image x, the DnCNN estimates the corresponding clean image y by applying the learned mapping function F: X → Y to x. This process can be represented by
y = F(x)
where x is the noisy image and y is the anticipated clean image. It is anticipated that the estimated clean picture y will be a denoised version of the noisy image x.

Eur. Chem. Bull. 2023, 12 (S3), 1518 – 1530

1524

minimize $\sum \|F(x) - y\|^2$

where y corresponds to the ground truth clean picture for an image that is noisy (x), and F(x) is the estimated clean image derived by the DnCNN, and $\|.\|^2$ represents the L2 norm.

During testing, given a noisy image x, the DnCNN estimates the corresponding clean image y by applying the learned mapping function F: X → Y to x. This process can be represented by

$$y = F(x)$$

where y is the estimated clean image, and x is the noisy image. The estimated clean image y is expected to be a denoised version of the noisy image x.

Transformation Enhancement In Mixed Pixel Region

The areas surrounding water bodies, including Lake and river, are improved in the Haar wavelet-processed image. Rivers like the River region and have clearly improved conditions. According to it is necessary to measure the limits apart from the coastal zone, of the regions with flora and water bodies. To identify the to Use vegetation and water features to separate the coastal region from the rest of the land area. The edges and curves must also be improved for analyzing the measurement error and geometric correction brought on by mixed pixels, the proposed TDyWT improvement algorithm includes algorithms like the Haar wavelet transformations, L*a*b color analysis, and non-uniform illumination removal. The comparison of error modeling for measurements of land with irregular shapes is shown in Table 1.

Parameters	Original image	Retrospective correction image	L*a*b space image	Haar image	Dyadic image
F-measure(%)	96.32323	101.00000	99.63867	96.07087	53.92518
Recall	1.00000	1.00000	1.00000	1.00000	1.00000
Precision	0.93359	1.00000	0.96900	0.90704	0.43795
MPM(91000)	4.97808	0.00000	0.94674	5.22496	169.46426
pF measure(%)	96.53222	102.00000	99.56786	97.08074	62.93568
PSNR	11.65743	Infinity	16.48702	12.37097	2.82628
Sensitivity	1.00000	1.00000	1.00000	1.00000	1.00000

Table 1 Error Modeling Measurements

(a)   (b)

Fig 5 (a) Noisy Input Image of Lake (b) Denoised Output Image of Lake.

Eur. Chem. Bull. 2023, 12 (S3), 1518 – 1530

1525

(a)   (b)   (c)   (d)
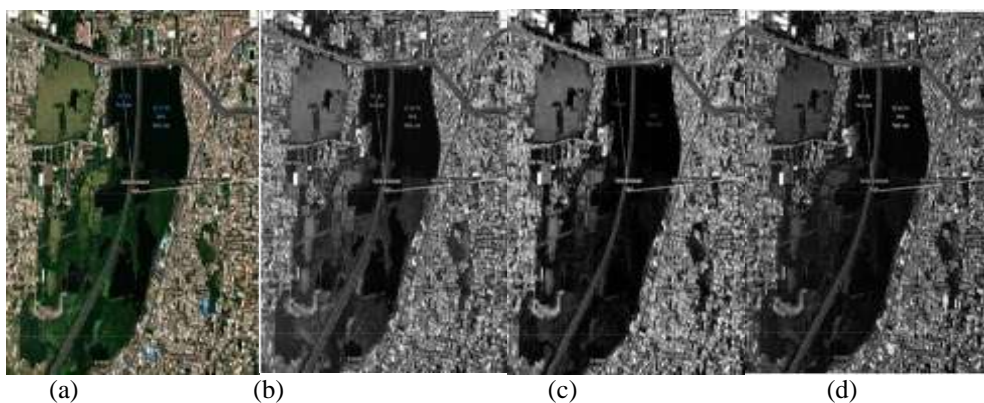Fig 6 (a) LANDSAT Satellite image (b) R-Band (c) G-Band (d) B-Band

(a)   (b)
Fig 7 (a) Noisy Input Image of River (b) Denoised Output Image of River

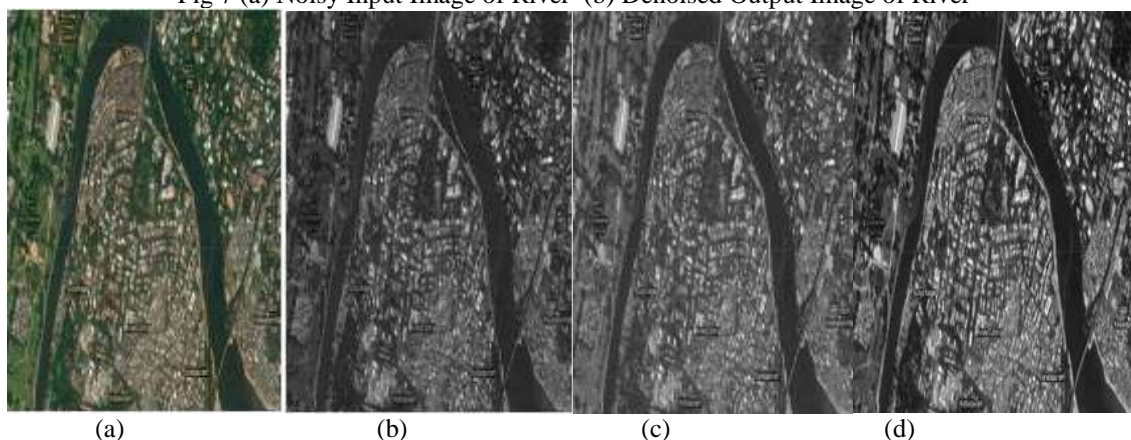(a)   (b)   (c)   (d)
Fig 8 (a) Input image from LANDSAT (b) Dyadic R-Band picture (c) Dyadic G-Band picture   (d)
Dyadic B-band image.

The aforementioned results contrast, however, with pixel improvement algorithms like the outcome of L*a*b color space, the image after enhanced retrospective rectification, and the image after DWT-Haar wavelet processing.

Enhancement In Mixed Pixel Region

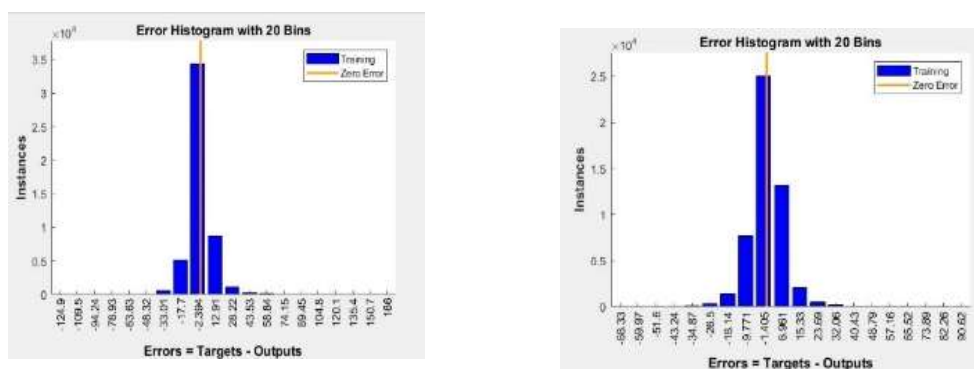Eur. Chem. Bull. 2023, 12 (S3), 1518 – 1530

1526

Fig 9 Error in Mixed pixel Region Enhancement

Enhancement in mixed pixel regions is a approach for enhancing visual quality in image processing of images that contain pixels with mixed or overlapping colors. A mixed pixel region occurs when a pixel in an image contains more than one color or texture due to the limitations of the sensor or the resolution of the imaging system.

There are several approaches to enhancing mixed pixel regions in images. One common technique is to use spectral un mixing, which separates the spectral signatures of the different materials or colors present in a mixed pixel region. This can be done using mathematical algorithms, such as linear spectral un mixing or non-negative matrix factorization.

Another approach is to use spatial filtering, which involves applying a filter to the image that smoothes out the mixed pixel regions and improves their overall appearance. This can be done using techniques such as median filtering, Gaussian filtering, or bilateral filtering.

In general, the goal of enhancement in mixed pixel regions is to enhance an image's overall visual appeal, making it simpler to perceive and evaluate. In fields like remote sensing, where photographs are used to study the Earth's surface and track environmental changes, this can be especially significant.

Area Measurement And Region Classification

For the purpose of measuring the land cover class area, the transverse dyadic wavelet transformed LANDSAT picture is used to count the number of pixels between two points. The multispectral LANDSAT-8 image has a 30 m per pixel resolution. In the LANDSAT image, there are 68.10 pixels between the two spots shown in Fig. 9a Also, as seen in Fig. 9b there are 68.96 pixels between each point in the TDyWT-processed image.

The two points in the LANDSAT image are separated by 2043 metres, while the two points in the TDyWT-processed image are separated by 2068 metres. Moreover, GPS ground truth verification confirms 2096 m and the TDyWT-processed image offers the greater accuracy.
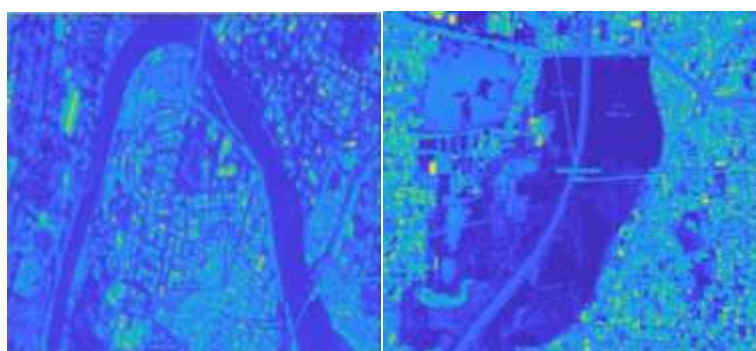

Fig 10 region classification in LANSAT Image.

Eur. Chem. Bull. 2023, 12 (S3), 1518 – 1530

1527
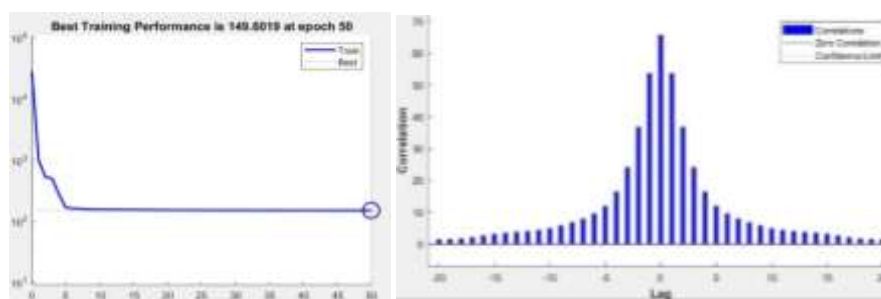
2. Result and analysis

Fig 11 Correlation of mixed pixels

We introduced related rank as a weight coefficient to the Feature Expansion Algorithm in order to achieve better results (RR). As seen in Fig 10 , we varied the values for RR in accordance with the separations between the target point and its neighboring points. The closest point receives the highest associated rank, whereas remote points are given a lower weight.
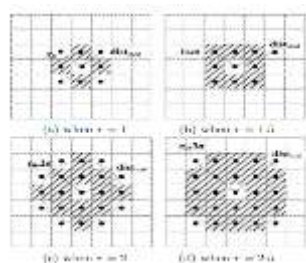

Fig 12 Region rank radius

A water body extraction model was developed using stacked sparse auto encoder (SSAE). The values from were chosen through a number of experiments to start the sparse auto encoder and soft max. Also, in order to improve accuracy, we implemented the Feature Extraction Algorithm and chose the simulation experiment software MATLAB (Matrix & Laboratory).

3. Conclusion

It is crucial for planning and development that vegetation and water bodies are identified and both urban and rural regions are measured in LANDSAT pictures. Nevertheless, the existing technique for categorizing and measuring vegetative and water bodies in the LANDSAT image is hampered by curvature and boundary effects of geometric distortion and mixed pixels is inaccurate. In contrast to hand surveying, we suggest the TDyWT method to categorize When mixed pixel and geometric distortion has been removed, the vegetation and water body may be measured more precisely. Also, the proposed methodology sub classifies in the hilly and agricultural area, different land classes perform better with regard to vegetation and water bodies. The identification and measurement of vegetation and water Planning and development need the identification of bodies in LANDSAT images of both urban and rural areas. Yet, the current technique for categorizing and estimating vegetative and water bodies in the LANDSAT image is imprecise due to curvature and edge effects of geometric distortion and mixed pixels. We advise using the TDyWT method instead of hand surveying to classify the vegetation and water body after removing mixed pixel and geometric inaccuracy and more precisely estimate the area. Also, the proposed methodology divides up vegetation and water features into separate types of land in the hilly and agricultural region, where it performs better.

4. References

M. Prabu, N. R. Shanker, A. Celine Kavida, E. Ganesh. "Geometric distortion and mixed pixel elimination via TDYWT image enhancement for precise spatial measurement to avoid land survey error modeling" , Soft Computing, 2020

P. Mani, S. RajendiranNagalingam, K. Celine Kavida, G. Elanchezhian. "Mixed pixel removal in north Tamil Nadu region for accurate area measurement" , Computational Intelligence, 2021

BingyangGuo, Kechen Song, Hongwen Dong, Yunhui Yan, ZhibiaoTu, Liu Zhu. "NERNet:

Noise Estimation and Removal Network for Image Denoising" , Journal of Visual Communication and Image Representation, 2020

Simulated Evolution and Learning" , Springer Science and Business Media LLC, 2014

Kyungsang Kim, Dufan Wu, Kuang Gong, Joyita Dutta, Jong Hoon Kim, Young Don Son, Hang Keun Kim, Georges El Fakhri, Quanzheng Li. "Penalized PET reconstruction using deep learning prior and local linear fitting" , IEEE Transactions on Medical Imaging, 2018

Hamdan, M.N.. "Comparison Of Various Basic Wavelets For The Analysis Of Flow-Induced Vibration Of A Cylinder In Cross Flow" Journal of Fluids and Structures, 199608

M. Chavez, F. Grosselin, A. Bussalb, F. De VicoFallani, X. Navarro-Sune. "Surrogate-Based Artifact Removal From Single-Channel EEG" , IEEE Transactions on Neural Systems and Rehabilitation Engineering, 2018

Ajaya Shrestha, ArunTimalsina. "Color image steganography technique using daubechies discrete wavelet transform" , 2015 9th International Conference on Software, Knowledge, Information Management and Applications (SKIMA), 2015

Arqub OA, Abo-Hammour Z (2014) Numerical solution of systems of second-order boundary value problems using continuous genetic algorithm. InfSci 279:396–415

Arqub OA, Al-Smadi M, Momani S, Hayat T (2016) Numerical solutions of fuzzy differential equations using reproducing kernel Hilbert space method. Soft Comput 20(8):3283–3302

Arqub OA, Al-Smadi M, Momani S, Hayat T (2017) Application of reproducing kernel algorithm for solving second-order, twopoint fuzzy boundary value problems. Soft Comput 21:7191–7206

Awrangjeb M, Fraser CS (2014) An automatic and threshold-free performance evaluation system for building extraction techniques from Airborne LIDAR data. IEEE J Sel Top Appl Earth Observ Remote Sens 7(10):4184–4198

Blaschke T, Feizizadeh B, Helbling D (2014) Object-based image analysis and digital terrain analysis for locating landslides in the Urmia Lake Basin, Iran. IEEE J Sel Top Appl Earth Observ Remote Sens 7(12):4806–4817

Bruzzone L, Carlin L (2006) A multilevel context-based system for classification of very high spatial resolution Images. IEEE Trans Geosci Remote Sens 44(9):2587–2600

Demirel H, Anbarjafari G (2010) Satellite image resolution enhancement using complex wavelet transform. IEEE Geosci Remote Sens Lett 7(1):123–126 Deng W, Zhao H, Zou L et al (2017a) A novel collaborative optimization algorithm in solving complex optimization problems. Soft Comput 21:4387–4398

Deng W, Zhao H, Yang X, Xiong J, Sun M, Li B (2017b) Study on improved adaptive PSO algorithm for solving multi-objective gate assignment. Appl Soft Comput 59:288–302

Deng W, Xu J, Zhao H (2019) An improved ant colony optimization algorithm based on hybrid strategies for scheduling problem. IEEE Access 7:20281–20292

Fan J, Chen T, Lu S (2015) Vegetation coverage detection from very high-resolution satellite imagery. In: 2015 Visual communications and image processing (VCIP), pp 1–4, 13–16 Dec 2015 Harbas I, Subasic M (2014) Detection of roadside vegetation using features from the visible spectrum. In: MIPRO 2014, Opatija, Croatia, pp 1204–1209, 26–30 May 2014 Iovan C, Boldo D, Cord M (2008) Detection, characterization, and modeling vegetation in urban areas from high-resolution aerial imagery. IEEE J Sel Top Appl Earth Observ Remote Sens 1(3):206–213

Lindberg E, Eysn L, Hollaus M, Holmgren J, Pfeifer N (2014) Delineation of tree crowns and tree species classification from full-waveform airborne laser scanning data using 3-D ellipsoidal clustering. IEEE J Sel Top Appl Earth Observ Remote Sens 7(7):3174–3181

Long Z, He M, Shi H, Rao R (2009) Study on water bodies extraction with FY3A satellite image. In: 2nd International congress on image and signal processing, 2009. CISP '09, pp 1–5, 17–19 Oct 2009

McInnes WS, Smith B, McDermid GJ (2015) Discriminating native and nonnative grasses in the dry mixedgrass prairie with MODIS NDVI time series. IEEE J Sel Top Appl Earth Observ Remote Sens 8(4):1395–1403

Nageswari CS, Prabha KH (2018) Preserving the border and curvature of fetal heart chambers through TDyWT perspective geometry wrap segmentation. Multimed Tools Appl 77(8):10235–10250

Pal M, Mather PM (2005) Support vector machines for classification in remote sensing. Int J Remote Sens 26(5):1007–1011

Paris C, Valduga D, Bruzzone L (2016) A hierarchical approach to three-dimensional segmentation of LiDAR data at single-tree level in a multilayered forest. IEEE Trans Geo Sci Remote Sens 54(7):4190–4203

Petrou ZI, Manakos I, Stathaki T, Mu¨cher CA, Adamo M (2015) Discrimination of vegetation height categories with passive satellite sensor imagery using texture analysis. IEEE J Sel Top Appl Earth Observ Remote Sens 8(4):1442–1455

Eur. Chem. Bull. 2023, 12 (S3), 1518 – 1530

1529

Shi H, Chen L, Bi F, Chen H, Yu Y (2015) Accurate urban area detection in remote sensing images. IEEE Geosci Remote Sens Lett 12(9):1948–1952 Singh K, Ghosh M, Sharma SR (2016) WSB-DA: water surface boundary detection algorithm using LANDSAT 8 OLI data. IEEE J Sel Top Appl Earth Observ Remote Sens 9(1):363–368

Sirmacek B, Unsalan C (2009) Urban-area and building detection using SIFT keypoints and graph theory. IEEE Trans Geosci Remote Sens 47(4):1156–1167

Sirmacek B, Unsalan C (2010) Urban area detection using local feature points and spatial voting. IEEE Geosci Remote Sens Lett 7(1):146–150 Wang Z, Boesch R (2007) Color- and texture-based image segmentation for improved forest delineation. IEEE Trans Geo Sci Remote Sens 45(10):3055–3062

Xie J, Jiang Y, Tsui H-T, Heng P-A (2006) Boundary enhancement and speckle reduction for ultrasound images via salient structure extraction. IEEE Trans Biomed Eng 53(11):2300–2309

Zarea A, Mohammadzadeh A (2016) A novel building and tree detection method From LiDAR data and aerial images. IEEE J Sel Top Appl Earth Observ Remote Sens 9(5):1864–1875

Zeng C, Wang J, Huang X, Bird S, Luce JJ (2015) Urban water body detection from the combination of high-resolution optical and SAR images. In: Joint urban remote sensing event (JURSE), pp 1–4

Zhan Z, Lai B (2012) Vegetation detection of close-range images for landslide monitoring. In: International conference on computer vision in remote sensing (CVRS), pp 13–18, 16–18 Dec 2012

Zhao H, Zheng J, Xu J, Deng W (2019a) Fault diagnosis method based on principal component analysis and broad learning system. IEEE Access 7:99263–99272 Zhao H, Liu H, Xu J, Deng W (2019) Performance prediction using high-order differential mathematical morphology gradient spectrum entropy and extreme learning machine. In: IEEE transations on instrumentation measurement. IEEE, pp 1–1. https://doi.org/10.1109/TIM.2019.2948414

Zhu H, Barish M, Pickhardt P, Liang Z (2013) Haustral fold segmentation with curvature-guided level set evolution. IEEE Trans Biomed Eng 60(2):321–33

Eur. Chem. Bull. 2023, 12 (S3), 1518 – 1530

1530